Sensitivity advantage of swept source and Fourier domain optical coherence tomography

Michael A. Choma, Marinko V. Sarunic, Changhuei Yang, Joseph A. Izatt

Department of Biomedical Engineering, Duke University, Durham, NC 27708
jizatt@duke.edu

Abstract: We present theoretical and experimental results which demonstrate the superior sensitivity of swept source (SS) and Fourier domain (FD) optical coherence tomography (OCT) techniques over the conventional time domain (TD) approach. We show that SS- and FD-OCT have equivalent expressions for system signal-to-noise ratio which result in a typical sensitivity advantage of 20-30dB over TD-OCT. Experimental verification is provided using two novel spectral discrimination (SD) OCT systems: a differential fiber-based 800nm FD-OCT system which employs deep-well photodiode arrays, and a differential 1300nm SS-OCT system based on a swept laser with an 87nm tuning range.

References and links

1. D. Huang, E. A. Swanson, C. P. Lin, J. S. Schuman, W. G. Stinson, W. Chang, M. R. Hee, T. Flotte, K. Gregory, and C. A. Puliafito, "Optical coherence tomography," Science **254**, 1178-1181 (1991).
2. A. F. Fercher, C. K. Hitzenberger, G. Kamp, and S. Y. Elzaiat, "Measurement of Intraocular Distances by Backscattering Spectral Interferometry," Opt. Commun. **117,** 43-48 (1995).
3. G. Häusler and M. W. Lindner, ""Coherence Radar" and "Spectral Radar"—New Tools for Dermatological Diagnosis," J. Biomed. Opt. **3**, 21-31 (1998).
4. M. Wojtkowski, R. Leitgeb, A. Kowalczyk, T. Bajraszewski, and A. F. Fercher, "In vivo human retinal imaging by Fourier domain optical coherence tomography," J. Biomed. Opt. **7**, 457-463 (2002).
5. M. Wojtkowski, A. Kowalczyk, R. Leitgeb, and A. F. Fercher, "Full range complex spectral optical coherence tomography technique in eye imaging," Opt. Lett. **27**, 1415-1417 (2002).
6. S. R. Chinn, E. A. Swanson, and J. G. Fujimoto, "Optical coherence tomography using a frequency-tunable optical source," Opt. Lett. **22**, 340-342 (1997).
7. B. Golubovic, B. E. Bouma, G. J. Tearney, and J. G. Fujimoto, "Optical frequency-domain reflectometry using rapid wavelength tuning of a Cr4+:forsterite laser," Opt. Lett. **22**, 1704-1706 (1997).
8. F. Lexer, C. K. Hitzenberger, A. F. Fercher, and M. Kulhavy, "Wavelength-tuning interferometry of intraocular distances," Appl. Opt. **36**, 6548-6553 (1997).
9. U. H. P. Haberland, V. Blazek, and H. J. Schmitt, "Chirp Optical Coherence Tomography of Layered Scattering Media," J. of Biomed. Opt. **3**, 259-266 (1998).
10. R. Leitgeb, C. K. Hitzenberger, and A. F. Fercher, "Performance of fourier domain vs. time domain optical coherence tomography," Opt. Express **11**, 889-894 (2003).
11. E. A. Swanson, D. Huang, M. R. Hee, J. G. Fujimoto, C. P. Lin, and C. A. Puliafito, "High-Speed Optical Coherence Domain Reflectometry," Opt. Lett. **17**, 151-153 (1992).
12. M. A. Choma, C. Yang, and J. A. Izatt, "Instantaneous quadrature low coherence interferometry with 3x3 fiber optic couplers," Accepted to Opt. Lett. (2003).
13. A. M. Rollins and J. A. Izatt, "Optimal interferometer designs for optical coherence tomography," Opt. Lett. **24**, 1484-1486 (1999).
14. S. U. Pillai, *Array Signal Processing* (Springer-Verlag, New York, 1989).
15. A. G. Podoleanu, "Unbalanced versus balanced operation in an optical coherence tomography system," Appl. Opt. **39**, 173-182 (2000).
16. C. Dorrer, N. Belabas, J. P. Likforman, and M. Joffre, "Spectral resolution and sampling issues in Fourier-transform spectral interferometry," J. Opt. Soc. Am. B **17**, 1795-1802 (2000).

1. Introduction

In the decade since its introduction, optical coherence tomography (OCT) has proven to be an important modality for micrometer-scale imaging [1]. To date, virtually all systems built for clinical and biological use have employed a variable group delay reference arm to coherently gate backscattered light from various depths in a sample. While successful, this time domain (TD) approach is hampered by the relatively complicated optical and mechanical designs needed to scan ~10ps delays at kilohertz rates in order to achieve real-time imaging.

An alternate approach to coherence gating that does not employ a scanning delay line involves acquiring as a function of optical wavenumber the interferometric signal generated by mixing sample light with reference light at a fixed group delay [2]. Two distinct methods have been developed that employ this spectral discrimination (SD) approach. The first, Fourier-domain OCT (FD-OCT) [2-5] uses a broadband light source and achieves spectral discrimination with a dispersive spectrometer in the detector arm. The second method, swept-source OCT (SS-OCT) [2,6-9], time-encodes wavenumber by rapidly tuning a narrowband source through a broad optical bandwidth. Until recently, it has been unclear how the performance of SD-OCT techniques compares with TD-OCT. A recently published work [10] demonstrated superior sensitivity (defined as the signal-to-noise ratio for a perfect sample reflector) of an FD-OCT implementation over TD-OCT. Here we demonstrate the general sensitivity advantage of SD-OCT techniques over TD-OCT techniques. We accomplish this by deriving and experimentally validating an SNR expression for SS-OCT and then by showing that SS-OCT and FD-OCT have equivalent SNR expressions.

2. Theoretical analysis

A fiber-based SS-OCT system is shown in Fig. 1(a). The ith photodetector output in the case of a single sample reflector is related to:

$$P_{Di}(k) = \left\langle \left| E_{Di}(k) \right|^2 \right\rangle = S(k)R_R + S(k)R_s + 2S(k)\sqrt{R_R R_S} \cos(2k\Delta x + \varphi_i). \tag{1}$$
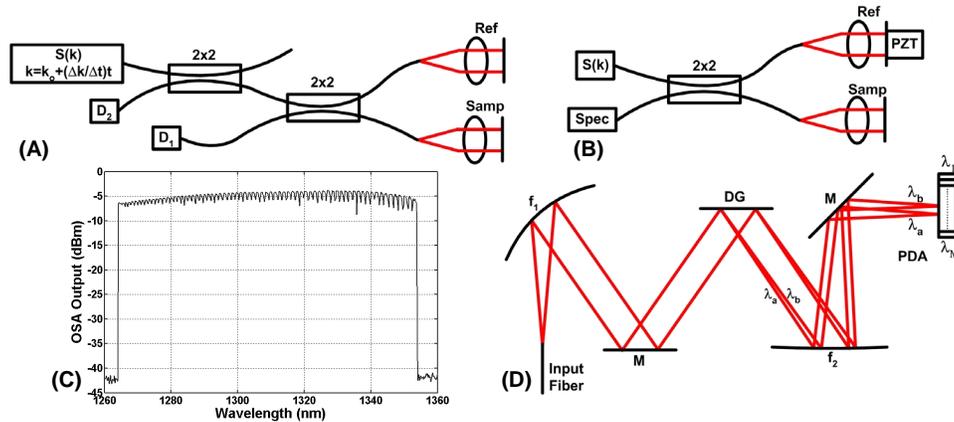

Fig. 1. A) Differential SS-OCT setup. The output of detectors 1 and 2 are differenced in software. B) Differential FD-OCT setup. Differential detection is accomplished by dithering the phase of the reference arm field by $180°$ with a piezo-mounted mirror on alternate scans. C) Swept source output measured with an optical spectrum analyzer (OSA). The apparent modulation appearing in the OSA plot is an artifact of spectral resolution and sweep time setting of the OSA. D) Czerny-Turner grating spectrometer (Spec) employed in FD-OCT system. D, detector; DG, diffraction grating; f, focal length of reflective optical element; M, mirror; PDA, photodiode array; PZT, piezoelectric actuator.

Here, k is optical wavenumber, $S(k)$ is the source spectral density (watts per wavenumber), Δx is the pathlength difference between the reference and sample arms, and R_R and R_S are the

reference and sample arm reflectivities, respectively. φ_i is the interferometric phase shift associated with the ith detector signal ($|\varphi_1-\varphi_2|=180°$). In the case of SS-OCT, $k=k_o+t(\Delta k/\Delta t)$, where t is time, k_o is the starting wavenumber, and Δt is the sweep, and therefore A-scan, time. Δk is the total optical bandwidth through which the narrowband source of linewidth Λ is swept.

In SS-OCT, the acquired signal ideally has values at M evenly spaced wavenumbers $K=\{k_1, k_2,...,k_M\}$ with wavenumber spacing $\delta k=\Delta k/M$. For SS-OCT, δk has a lower limit of Λ. The sampled SS-OCT signal from the ith detector, $D_i[k_m]$, is thus

$$D_i[k_m]=\frac{1}{2^i}\rho\,S[k_m]\Big(R_R+R_S+2\sqrt{R_R R_S}\,\cos(2k_m\Delta x+\varphi_i)\Big).\tag{2}$$

Here, $m\in\{1,M\}$, ρ is the detector responsivity and $S[k_m]$ is the sample illumination power $\frac14\Lambda\ S(k_m)$.

The aim of SS-OCT is to obtain a depth-reflectivity profile $D[x_n]$ of the sample arm. This can be obtained by discrete Fourier transforming any $D_i[k_m]$ to obtain [2]

$$D[x_n]=\sum_{m=1}^{M}D_i[k_m]\mathrm{Exp}[-j2k_m x_n].\tag{3}$$

The factor of 2 in the kernel exponent ensures the recovery of single-sided distances, and $n\in\{1,M\}$. In the x-domain, the channel spacing is $\delta x=\pi/\Delta k$ and the scan depth is $\Delta x_{max}=\pi/\delta k$ [$-\pi/(2\delta k)$ to $+\pi/(2\delta k)$]. Because $D[k_m]$ is real-valued, Eq. (3) yields an A-scan in which $D[+x]$ and $D[-x]$ are complex conjugate pairs. Thus, the effective scan depth is $\Delta x_{max}=\pi/(2\delta k)$. The design equation for the number of samples is $M=2\Delta x_{max}\Delta k/\pi$, giving typical values of $M\sim10^2$-10^3. The A-scan axial resolution is $4\ln2/\Delta k_{fwhm}$ using a Gaussian source with a full width-half maximum bandwidth Δk_{fwhm} [11], while the resolution is $\pi/\Delta k$ using a rectangular source. Qualitatively, Eq. (3) has three peaks in the case of a single sample reflector. One peak represents the Fourier transform of $S(k)$, and is centered at x=0. The two other peaks sit at $x_n=\pm\Delta x$, and are due to the interferometric portion of Eq. (3).

The source spectral shape at $x=0$ and the complex conjugate ambiguity in the Fourier transform of $D[k_m]$ can be eliminated by retrieving the complex interferomeric signal via phase-stepping [5], polarization quadrature encoding, or the use of NxN (N>2) fiber couplers [12]. $D[x_n]$ is thus given by:

$$D[x_n]=\sum_{m=1}^{M}\Big[\big(D^0[k_m]-D^{\mathrm{DC}}[k_m]\big)+j\big(D^{90}[k_m]-D^{\mathrm{DC}}[k_m]\big)\Big]\mathrm{Exp}[-j2k_m x_n].\tag{4}$$

The superscripts 0 and 90 of $D[k_m]$ refer to the phase difference in degrees between the reference and sample arm fields, while the DC superscript refers to spectral shape, autocorrelation, and source noise terms that must be removed for complex signal retrieval [5]. $D^{\mathrm{DC}}[k_m]$ is defined as $D^0[k_m]+D^{180}[k_m]$. The differential topology in Fig. 1(a) only allows for the retrieval of the real part of Eq. (4):

$$D[x_n]=\sum_{m=1}^{M}\left(\frac{1}{2}D_1[k_m]-D_2[k_m]\right)\mathrm{Exp}[-j2k_m x_n].\tag{5}$$

The sensitivity analysis that ensues will use A-scans obtained from the Fourier transform of $D_1[k_m]$ [i.e., Eq. (3), $i=1$]. This analysis readily can be extended to differential, phase stepping, and NxN topologies. For example, the sensitivity of a differential A-scan from Fig. 1(a), Eq. (5) is identical to that obtained from Eq. (3), $i=1$ because the signal lost by halving $D_1[k_m]$ is regained in $D_2[k_m]$, whose magnitude is half of that of $D_1[k_m]$.

In the case of a single sample reflector located at Δx, the peak value of the interferometric portion of the A-scan is:

$$D[x_n=\pm\Delta x]=\frac{1}{2}\rho\sqrt{R_R R_S}\sum_{m=1}^{M}S[k_m]=\frac{1}{2}\rho\sqrt{R_R R_S}\,S_{ssoct}.\tag{6}$$

S_{ssoct} is the summation of $S[k_m]$ over all m. Just as the sample exposure in TD-OCT systems S_{tdoct} is constrained by ANSI exposure limits, so is $S[k_m]$, the instantaneous sample exposure

in SS-OCT systems. As such, $S_{ssoct} \approx M\, S_{tdoct}$. Eq. (6) can be though of as the coherent addition of M waves of amplitude $\frac{1}{2}\rho(R_R R_S)^{1/2}S[k_m]$.

In order to calculate the signal-to-noise (SNR) of SS-OCT, we first must address the issue of how noise transforms from the k-domain to the x-domain. $D[k_m]$ can be generalized to include an additive, uncorrelated Gaussian white noise term $\alpha[k_m]$. $\alpha[k_m]$ has a mean of zero, a standard deviation $\sigma[k_m]$, and a lower limit set by shot noise. In OCT systems, it is typical for $R_R \gg R_S$. Thus, in the shot noise limit, $\sigma[k_m]=(2e\mathrm{D}[k_m]B_{ssoct})^{1/2}$, where e is electronic charge and B_{ssoct} is the noise equivalent bandwidth of the system [13]. In contrast to Eq. (6), the value of $\alpha[x_n]$ is arrived at by incoherently adding M waves of amplitude $\alpha[k_m]$ [14].Because the noise adds in intensity,

$$\sigma_x = \sqrt{\sum_{m=1}^{M}\sigma^2[k_m]} = \sqrt{e\rho\, R_R\, S_{ssoct}\, B_{ssoct}} \; , \qquad (7)$$

where σ_x is the standard deviation of each pixel in x-space. We are guaranteed that σ_x is a constant so long as $\sigma[k_m]$ is white. The SNR of SS-OCT, SNR_{ssoct}, is thus

$$\mathrm{SNR}_{ssoct} = \frac{\rho\, R_S\, S_{ssoct}}{4\,e\,B_{ssoct}} \approx M\,\frac{\rho\, R_S\, S_{tdoct}}{4\,e\,B_{ssoct}} \; . \qquad (8)$$

Since $\mathrm{D}[k_m]\propto\cos(2t\Delta x\Delta k/\Delta t)$, as Δx increases, the electronic bandwidth of $\mathrm{D}[k_m]$ also increases. Moreover, the bandwidth of $\mathrm{D}[k_m]$ limits the effective scan depth of $\mathrm{D}[x_n]$. The bandwidth of $\mathrm{D}[k_m]$ is limited by the analog-to-digital sampling frequency $f_s=M/\Delta t=2\Delta k\Delta x_{max}/(\pi\Delta t)$. Since the photodetector output is low-pass filtered at one-half the sampling frequency to prevent the aliasing of high-frequency noise, $B_{ssoct}=\Delta k\Delta x_{max}/(\pi\Delta t)$.

In order to compare this result with time domain OCT, we need to compare Eq. (8) with the accepted SNR expression for TD-OCT [11]

$$\mathrm{SNR}_{tdoct} = \frac{\rho\, R_S\, S_{tdoct}}{2\,e\,B_{tdoct}} \; . \qquad (9)$$

Assuming a Gaussian source, $B_{tdoct}=2\Delta k_{fwhm}\Delta x_{max}/(\pi\Delta t)$ [11]. Since $\Delta k=2\Delta k_{fwhm}$, $B_{tdoct}=B_{ssoct}$, and since $S_{ssoct}=\frac{1}{2}MS_{tdoct}$ for a Gaussian source, we expect SS-OCT to be $\frac{1}{4}M$ times more sensitive than TD-OCT. For a rectangular spectral source, $B_{tdoct}=B_{ssoct}$ and $S_{ssoct}=MS_{tdoct}$, so the sensitivity advantage is $\frac{1}{2}M$. Overall, this translates into a sensitivity advantage of 20-30dB over TD-OCT.

Because both S_{ssoct} and B_{ssoct} scale linearly with M, the sensitivity of swept-source OCT is independent of both scan depth and source bandwidth. This is in sharp contrast to time-domain where the sensitivity is inversely proportional to both scan depth and bandwidth. This relationship is graphically represented in Fig. 2.
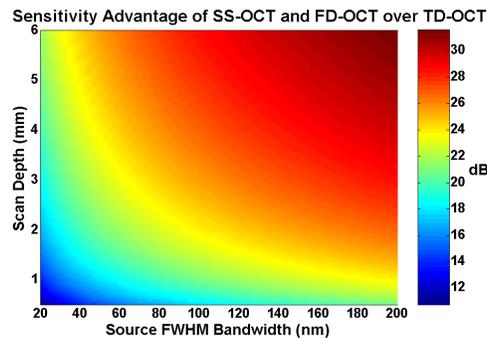

Fig. 2. Sensitivity advantage of SS-OCT and FD-OCT over conventional TD-OCT with a Gaussian source at 1300nm. Sensitivity advantage is defined as $\mathrm{SNR}_{sdoct}/\mathrm{SNR}_{tdoct}$ and expressed in dB.

The derivation of the SNR expression for FD-OCT from this analysis is straightforward. As with SS-OCT, the FD-OCT signal is discrete in wavenumber. This discretization occurs at a detector arm spectrometer that spectrally disperses the light onto M detectors. This generates M spectral channels of width $\delta k = \Delta k/M$. Assuming for the purpose of comparison that FD-OCT employs the same source used in TD-OCT, $S_{fdoct} = S_{tdoct} \approx S_{ssoct}/M$. However, the bandwidth of FD-OCT is determined by the detector integration time, which is Δt, the entire A-scan time. Thus, $B_{fdoct} = B_{ssoct}/M$. This is consistent with the recent analysis of Leitgeb et. al. [10]. As with SS-OCT, the sensitivity advantage of FD-OCT over TD-OCT is independent of source bandwidth and scan depth (Fig. 2). A general expression for the sensitivity of SD-OCT is

$$\mathrm{SNR}_{sdoct} = \frac{\rho \, S \, R_S \, \Delta t}{2e} . \tag{10}$$

In FD-OCT, S is the source power. In SS-OCT, it is the mean value of $S[k_m]$ (i.e., S_{ssoct}/M). We thus conclude that both FD-OCT and FD-OCT are 20-30dB more sensitive than TD-OCT is.

It is important to note that the theoretical SNR gain of SS-OCT and FD-OCT compared to TD-OCT derived above rests upon the assumption of shot noise-limited detection in each detection channel. As has been addressed in previous publications for the case of TD-OCT, achievement of this limit requires sufficient reference arm power to assure shot noise dominance, but usually requires significant reference arm attenuation to minimize excess noise [13, 15]. In the case of SS-OCT, the SNR of the spectral domain interferometric signal output by the photodetector is equal to the SNR of a time-domain OCT system photodetector output operating at the same line rate and reference arm power, thus the optimal reference arm power level for SS-OCT is expected to be similar to that for TD-OCT. In FD-OCT, where the reference arm power is dispersed onto M photodetectors, the total reference power required to achieve shot noise-limited detection on all receivers simultaneously is more than that required for SS-OCT and TD-OCT by a factor of M. However, whether or not this requires re-design of the interferometer coupling ratio depends upon the desired A-scan rate and the noise performance of the detectors used, which may be more favorable in the case of intrinsically low readout noise devices such as CCD arrays.

3. Experimental results

In order to verify this SD-OCT sensitivity analysis, we constructed differential SS-OCT and FD-OCT systems. The SS-OCT setup is in Fig. 1(a). This differential interferometer topology allows for the cancellation of DC, excess noise, and autocorrelation terms which otherwise contaminate SD-OCT images. The swept laser source (Micron Optics, Inc.) featured an average output power of ~2mW, a sweep time of 3.5ms, center wavelength λ_o=1308nm, and sweep bandwidth $\Delta\lambda$=87nm (Fig. 1(c)). The detector photocurrents were sampled using a 12-bit A/D converter at f_s=62 KHz, giving M=217 and Δx_{max}=1.1 mm. With 500μW incident on the sample and 47dB of calibrated sample arm attenuation, 121 dB of SNR was measured for the peak at 0.2mm (Figs. 3(a), 4). The SNR in dB was calculated as twenty time the base-10 logarithm of the ratio of the A-scan peak height to the standard deviation of the noise floor. The noise floor standard deviation was taken at the location of the A-scan peak by blocking the sample arm. This is significantly higher than the TD-OCT SNR of 107 dB predicted from Eq. (9), and is consistent with the 126 dB of SNR predicted by Eq. (10). A system resolution of 10μm was measured. The signal drop-off and peak broadening observed at deeper reflector positions (Fig. 3(a)) were due to nonlinearities in the wavenumber scan. This fall-off phenomenon previously has been observed in SS-OCT [7] and in FD-OCT [4], and may be addressed by numerically resampling the data to correct for these nonlinearities [16]. In principle, the finite linewidth of the swept source can contribute to fall off just as the finite pixel width of FD-OCT array detectors do [10]. However, so long as the source linewidth is much narrower than the spectral channel width δk, this source of fall-off is avoided.
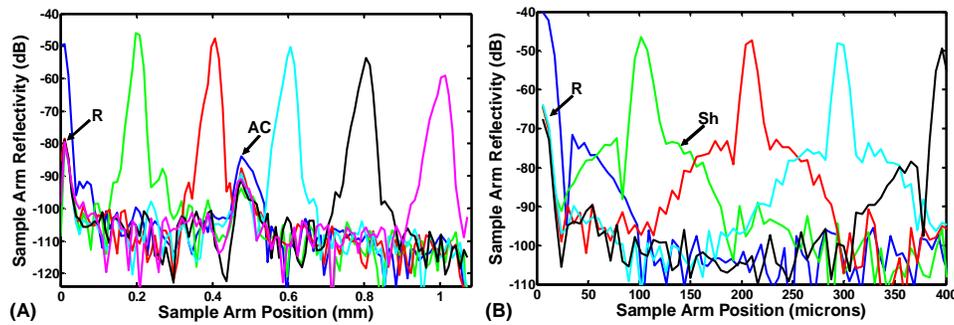
Fig. 3. A) SS-OCT peaks from a calibrated -47dB reflector at 200μm spacing increments. B) FD-OCT peaks from a calibrated -38dB reflector at 100μm increments. The shoulders (Sh) are artifacts of interpolation of the data from wavelength to wavenumber [16]. Imperfections in software differencing lead to residual DC (R) and autocorrelation (AC) peaks.

Our fiber-based FD-OCT system is illustrated in Fig. 1(b). The light source used was a superluminescent diode with λ_o=826 nm and $\Delta\lambda$=24.5 nm. A Czerny-Turner grating spectrometer (Fig. 1(d)) was used in conjunction with a 1024 element NMOS silicon photodiode array detector (PDA) with a specified well depth of 156 million electrons/pixel. The A-scan acquisition rate was 200 Hz (Δt=5ms). Data was resampled from wavelength to wavenumber with a cubic spline algorithm. We used data from the M=488 illuminated PDA elements that represented twice the FWHM optical spectrum. The reference mirror was mounted on a piezoelectric transducer and calibrated for 180° of rapidly addressable phase delay under computer control.

With 220 μW incident on the sample and a calibrated 38 dB of calibrated sample arm attenuation, a system sensitivity of 106dB (Figs. 3(b), 4) was measured. This is higher than the maximum sensitivity for a time-domain OCT system with identical parameters of 104dB (Eq. (9)), although it is also substantially less than the predicted sensitivity for a Fourier-domain OCT system of 126 dB (using Eq. (10)). We attribute the latter deficiency to approximately 16 dB of optical inefficiencies in our system (4 dB measured recoupling inefficiency in the sample arm and 12 dB measured optical inefficiency in the spectrometer). Although this FD-OCT system is clearly not optimized, the fact that we measured a system sensitivity in excess of the accepted shot-noise limit for time-domain OCT systems is convincing evidence that FD-OCT has significantly superior sensitivity. The free-space FWHM interferogram width was measured to be 14μm.

	TD-OCT Predicted	SD-OCT Predicted	Obs. SD-OCT SNR With ND Filter	Obs. SD-OCT SNR + Add'l Measured Losses
SS-OCT	107 dB	126 dB	120 dB	121 dB
FD-OCT	104 dB	126 dB	106 dB	122 dB

Fig. 4. Comparison of predicted TD-OCT SNR to predicted and experimental SNR of SD-OCT. The additional losses in the final column include measured recoupling inefficiencies in the sample arm and spectrometer losses. All predicted SNR values assume shot noise-limited detection. The TD-OCT predicted is based on a setup per reference 11. Briefly, it is a 2x2 fiber coupler-based Michelson interferometer with a broadband SLD source, a scanning reference arm mirror, and a single photodetector. The splitting ratio of the 2x2 coupler is 50%.

4. Conclusions

In conclusion, we have demonstrated the superior sensitivity of SS-OCT and FD-OCT as compared to TD-OCT. These results should further motivate the development of SS-OCT and FD-OCT engines for medical and biologic applications. Because the SNR of spectrally discriminated techniques are independent of the source coherence length, these methods should be particularly attractive to ultrahigh resolution OCT, where TD-OCT forces an inverse relationship between axial resolution and SNR.

Acknowledgements